

Identifying high-energy electronic states of NV^- centers in diamond

Minh Tuan Luu,^{1, a)} Christopher Linderälv,^{2, a)} Zsolt Benedek,^{3, 4, a)} Ádám Ganyecz,^{5, 4} Gergely Barcza,^{5, 4} Viktor Ivády,^{3, 4} and Ronald Ulbricht¹

¹⁾Max-Planck Institut für Polymerforschung, Ackermannweg 10, 55128 Mainz, Germany

²⁾University of Oslo, Department of Physics, Centre for Material Science and Nanotechnology, P.O. Box 1048, Blindern, Oslo N-0316, Norway

³⁾Department of Physics of Complex Systems, Eötvös Loránd University, Egyetem tér 1-3, H-1053 Budapest, Hungary

⁴⁾MTA–ELTE Lendület "Momentum" NewQubit Research Group, Pázmány Péter, Sétány 1/A, 1117 Budapest, Hungary

⁵⁾HUN-REN Wigner Research Centre for Physics, PO Box 49, H-1525, Budapest, Hungary

(*Electronic mail: ulbricht@mpip-mainz.mpg.de)

(*Electronic mail: ivady.viktor@tk.elte.hu)

(Dated: March 7, 2025)

The negatively charged nitrogen-vacancy center in diamond is a prototype photoluminescent point defect spin qubit with promising quantum technology applications, enabled by its efficient optical spin polarization and readout. Its low-lying electronic states and optical spin polarization cycle have been well characterized over decades, establishing it as a benchmark system for state-of-the-art computational methods in point defect research. While the optical cycle is well understood, a comprehensive energetic analysis of higher-lying states has received less attention until recently. In this joint experimental theoretical study, we identify and characterize five high-energy states beyond those involved in the optical cycle. Using transient absorption spectroscopy, we determine their transition energies and relative oscillator strengths. Additionally, we perform two independent numerical studies employing two state-of-the-art post-DFT methods to support the experimental findings and assign energy levels. These results enhance our understanding of the NV center's energy spectrum and providing a broader reference for benchmarking high-level first-principles methods.

Nitrogen-vacancy (NV) centers in diamond¹ have emerged as a promising platform for quantum sensing^{2–4} and quantum information processing.⁵ The negatively charged state (NV^-) is of particular interest due to its long spin coherence time at room temperature⁶ and the ability to optically initialize and read out spin states,¹ allowing measurements of physical quantities such as electromagnetic fields,⁷ temperature,⁸ and mechanical strain.⁹ Additionally, nearby nuclear spins enable the implementation of small-scale quantum computing circuits, while NV^- center implemented spin-photon interfaces and quantum repeaters hold promise for building quantum networks.

The spin-dependent optical excitation cycle, which enables optical initialization and readout, is governed by the low-lying electronically excited states of NV^- . These states, along with their optical and spin-orbit coupling, have been thoroughly studied, leading to a solid understanding of the spin polarization mechanism and the spin-dependent photoluminescence signal,¹⁰ making this defect has become a benchmark system for state-of-the-art theoretical methods.^{11–26} Higher-lying excited states, which can play a role in photoionization and photoelectric readout of NV^- ,²⁷ as well as extend the scope for theoretical benchmarking, have received much less attention.

Recently, we experimentally discovered a range of high-energy excited states using transient absorption (TA) spectroscopy.^{28,29} Our results also provided direct evidence of electron transfer from NV^- to nearby nitrogen defects, explaining photoluminescence quenching and its dependence

on nitrogen concentration.²⁸ Theoretical predictions for high-energy states have been scarce,^{19,30–33} making their identification difficult. This is also because standard computational methods have difficulties in dealing with excited states, especially those beyond the first excited state that are potentially resonant with the conduction band (CB). The situation has improved with the development of new post-density functional theory (DFT) methods that can simultaneously account for the static correlation of the localized defect states and the screening effect of the embedding host electron states.

In this Letter, we further investigate the newly observed excited state by experimentally determining the relative transition strengths and conducting state-of-the-art numerical simulations using two independent methods to identify and label features of the high-energy spectra.

A two-pump femtosecond TA setup was implemented to measure the excited electronic states of NV^- in both the triplet and singlet spin channels, shown schematically in Fig. 1a. The first pump has a photon energy of 2.4 eV (515 nm), followed by a second pump at 1.38 eV (900 nm) arriving 15 ns later. The white-light (WL) probe beam is generated in a 4 mm c-cut sapphire crystal, with a spectrum covering either the 1.5 - 3.3 eV range (2.4 eV input, for higher excited states measurements) or the 1.1 - 2.3 eV range (1.07 eV input, for lower singlet states measurements). We probe the change in the transmission of the WL pulse ($\Delta T/T$) under excitation, where $\Delta T/T > 0$ indicates either ground state bleaching (GSB) or stimulated emission (SE) from the excited state, while $\Delta T/T < 0$ signifies excited state absorption (ESA). To probe the triplet channel, the WL measures $\Delta T/T$ 5 ps after the first pump (2.4 eV). To measure the singlet channel, the system is al-

^{a)}These authors contributed equally

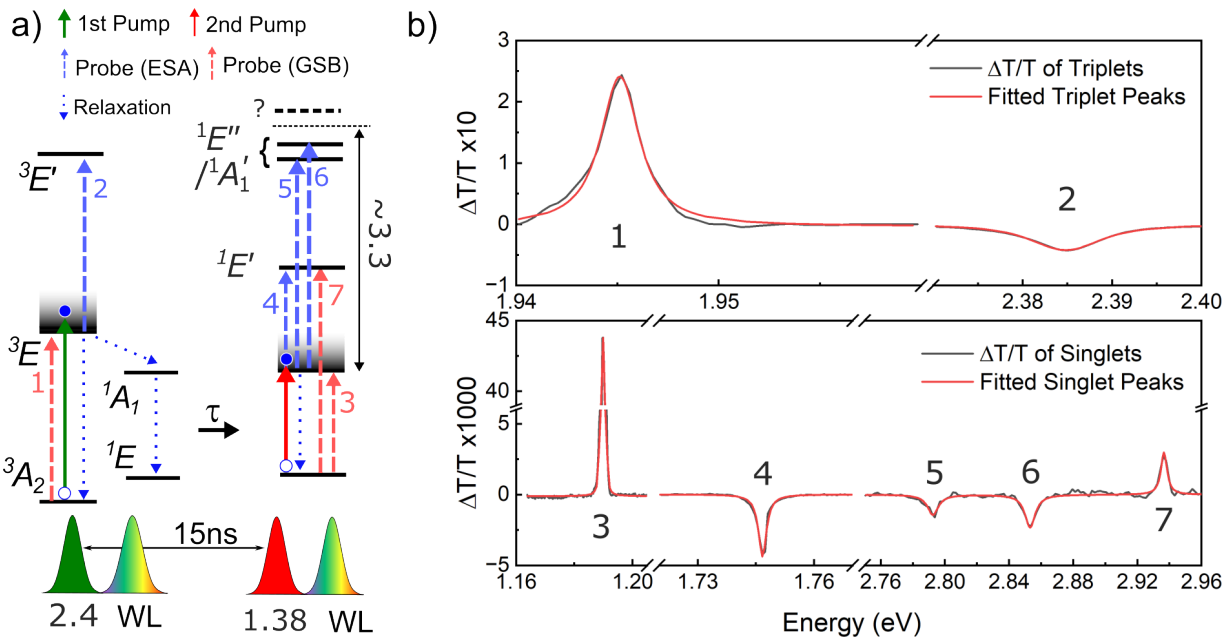


Figure 1. a) Schematic energy level structure and scheme of the TA measurements in triplet and singlet channels. Probe energy is limited to 3.3 eV from ¹A₁. b) Fitted curves of baseline-subtracted TA signal of transitions involving high energy states in NV⁻. Top: triplet channel; Bottom: singlet channel. Fit values are detailed in Table I.

lowed to relax after 2.4 eV excitation for 15 ns, so that population has either decayed to ³A₂ or ¹E. The second pump at 1.38 eV then excites the ¹E → ¹A₁ transition, with the white-light probing ΔT/T 5 ps later.

We used HPHT diamonds that contain about 2ppm of NV⁻ with a high concentration of single-substitutional nitrogen N_s (~100 ppm) to minimize the presence of NV⁰. All measurements were performed at a temperature of 10 K. Details of the experimental setup were previously published.²⁸

To theoretically describe the observed high-energy states two approach was used: (i) complete active space self-consistent field (CASSCF) method^{34–36} followed by 2nd-order N-electron valence state perturbation theory (NEVPT2)^{37–39} method on hydrogen-terminated nanodiamonds; (ii) constrained random phase and full-configurational interaction (cRPA+FCI) calculations^{17,40} on supercells.

The first methodology is similar to that described in detail in our previous work.²⁶ The used nanodiamonds, labeled as MODEL-I, MODEL-II, and MODEL-III, contain 34, 70, and 164 C atoms, and differ from our previous models²⁶ by that they are expanded to reduce the steric clash among terminal H atoms. State-average (SA) CASSCF calculations, followed by NEVPT2, were performed with the 4 defect-localized band-gap orbitals and 6 electrons in the active space, with 5 triplet and 8 singlet eigenstates. We applied the cc-pVDZ⁴¹ basis set along with def2/J⁴² and cc-pVDZ/C⁴³ auxiliary sets for density fitting approximations.^{44–46} The cluster geometries were optimized to the ground triplet (³A₂) electronic state also with CASSCF. CASSCF-NEVPT2 calculations were carried out using ORCA 6.0.1.^{47–49} See SI, section S1.4 for sample input files. Here, results with MODEL-III are presented, further results with smaller models are also in the SI.

The second method is using DFT and constrained random phase approximation (cRPA) to parameterize a Hamiltonian that can be solved using full configuration interaction (FCI). This method was demonstrated for the low-energy states of the NV⁻ center recently.⁴⁰ The cRPA+FCI calculations¹⁷ were performed as outlined in Ref. 40 using VASP^{50,51} and an in-house implementation of configuration interaction. Here, the lattice parameter was 3.57 Å and a 3 × 3 × 3 repetition of the unit cell was used for modeling the defect, consisting of 216 atoms. The exchange-correlation functional used was HSE06.^{52,53} The Brillouin zone was sampled at the Γ-point only and the plane wave basis was truncated at 520 eV. In the cRPA⁵⁴ calculation, 4 localized (spin-paired) states were used and empty states with energies up to 36 eV above the CB were included. The one-body matrix elements were obtained from orbital energy levels with Hartree double counting correction.⁴⁰

Figure 1 shows the energy scheme of the electronic states and optical transitions in both the singlet and triplet channels. Exciting electrons from ³A₂ to ³E using a 2.4 eV pump revealed an ESA feature at 2.38 eV (520 nm) whose relaxation dynamics matched that of the SE signal from the ³E state, indicating that the ESA signal observed is a spin-triplet state above ³E and was attributed to the ³E' state. This ³E' state also appeared in photoluminescence excitation (PLE) measurements⁵⁵ as a reduction of the NV⁻ PL signal and an increase in NV⁰ signal, hinting towards a charge conversion process as the ³E' got excited.

For the singlet system, the TA spectrum reveals several absorption peaks at 1.75 eV, 2.79 eV and 2.85 eV that share the relaxation lifetime of 130 ps of the ¹A₁ state.^{28,56} The spectrum also shows the ¹E → ¹E' transition at 2.94 eV as GSB.

Although 1.75 eV has been predicted before^{32,57,58} and experimentally verified along with a GSB replica at 2.94 eV,²⁸ the higher energy singlet states have neither been theoretically considered nor concretely observed experimentally. Due to the rapidly diminishing probe sensitivity towards the UV region, any potential transition located 3.3 eV above 1A_1 can not be identified.

All ZPL peaks were fitted with Lorentzian functions, giving their spectral positions, linewidth, and relative intensity. The intensity of the peaks in the triplet or singlet channel was normalized to the transition between the two lowest states in each system ($^3A_2 \rightarrow ^3E$ for triplets and $^1E \rightarrow ^1A_1$ for singlets). The results of the peak fitting are summarized in Table I alongside the values from theoretical models. Due to the low intensity of the higher singlet state peaks, the phonon sideband of such transitions could not be observed. The intensity of the peaks at the ZPLs comprises both the GSB and SE signals. However, this was only relevant in the $^3A_2 \rightarrow ^3E$ transition since the SE signal for this transition was comparable to the GSB signal. For other transitions, the SE signals were extremely low compared to the GSB signal or simply not detectable and thus excluded in the oscillator strength values.

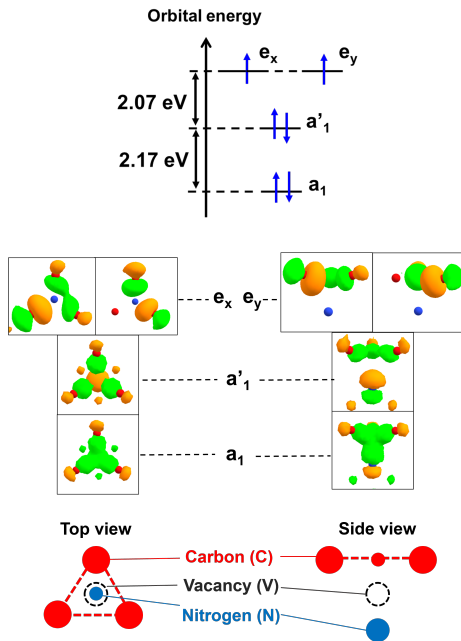


Figure 2. Top: Relative energy levels of the defect-localized orbitals of NV^- , as obtained upon wannierization, i.e. projection of localized spin paired HSE06 orbitals of the supercell model on sp^3 states of the nearest neighbour atoms. Bottom: surface plot of the localized band-gap orbitals in the vicinity of the vacancy. Green and orange surfaces indicate positive and negative wavefunction sign, respectively. (Note that CASSCF on cluster models provides similar defect orbital diagram.)

We start the theoretical considerations by discussing the possible nature of high-energy states using group theory, based on the orbital energy diagram of the NV^- center (see Fig. 2). There are four defect-localized orbitals in the vicinity of the band gap, formed by the superposition of four dangling

Triplet states (S=1)	E	Singlet states (S=0)		
		$\uparrow\uparrow$ \uparrow $-$ $^1A_1''$	$a_1 \rightarrow e$ $a_1 \rightarrow e$	
$\uparrow\uparrow$ \uparrow \uparrow 3A_1		$\uparrow\uparrow$ $\uparrow\uparrow$ $\uparrow - \uparrow$ $\uparrow \uparrow$ $^1A_1'$	$a_1' \rightarrow e$ $a_1 \rightarrow e$	2nd order excitations
Expected additional states		$\uparrow\uparrow$ $-$ \uparrow $^1A_1'$	$a_1' \rightarrow e$ $a_1' \rightarrow e$	
$\uparrow\uparrow$ $\uparrow\uparrow$ \uparrow \uparrow \uparrow \uparrow $^3E_x'$ $^3E_y'$		$\uparrow\uparrow$ $\uparrow\uparrow$ $\uparrow\uparrow$ $\uparrow\uparrow$ $\uparrow - \uparrow$ $\uparrow - \uparrow$ $\uparrow \uparrow$ $\uparrow \uparrow$ $^1E_x''$ $^1E_y''$	$a_1 \rightarrow e$	1st order excitations
$\uparrow\uparrow$ $\uparrow\uparrow$ \uparrow \uparrow \uparrow \uparrow 3E_x 3E_y		$\uparrow\uparrow$ $\uparrow\uparrow$ $\uparrow\uparrow$ $\uparrow\uparrow$ $\uparrow - \uparrow$ $\uparrow - \uparrow$ $\uparrow \uparrow$ $\uparrow \uparrow$ $^1E_x'$ $^1E_y'$	$a_1' \rightarrow e$	
Spin polarization cycle		$- \uparrow \uparrow -$ $\uparrow \uparrow \uparrow$ $\uparrow \uparrow \uparrow$ 1A_1	$e \rightarrow e$	0th order excitations
$\uparrow\uparrow$ \uparrow \uparrow 3A_2		$\uparrow\uparrow$ $\uparrow\uparrow$ $- \uparrow \uparrow -$ $\uparrow - \uparrow$ $\uparrow - \uparrow$ $\uparrow \uparrow$ $\uparrow \uparrow$ 1E_x 1E_y		

Figure 3. Expected electron configurations for the distribution of 6 electrons on the 4 band-gap orbitals according to group theory. The configurations are ordered - from bottom to top - according to the expected energy levels based on the orbital energy diagram.

atomic $2p$ orbitals around the vacancy. Using notations corresponding to the C_{3v} symmetry, we have two half-occupied degenerate e orbitals and two occupied a_1 orbitals (a_1 and a_1') in the ground state ~ 2 eV apart from each other. If we assume that all band-gap electronic states of NV^- are formed by excitations within the latter four orbitals, 5 triplet and 10 singlet excited states are conceivable in addition to 3A_2 , see Fig. 3.

In the bottom row, we show the occupation patterns where the e and a_1 orbitals are semi- and doubly occupied, respectively. These can be understood as "zeroth-order" excitations, which are expected to have the lowest energy level among all states. These states are 3A_2 , 1E , and 1A_1 .

For first-order excitations only $a_1' \rightarrow e$ and $a_1 \rightarrow e$ electron jumps are feasible and the orbital energy gap in the former case is approximately twice smaller. The $a_1' \rightarrow e$ process leads to 3E and $^1E'$ excited states. Among these, 3E is responsible for the 1.945 eV emission line of NV^- ⁵⁹ and is known to be involved in its spin polarization cycle¹⁰ ($^3A_2 \rightarrow ^1A_1 \rightarrow ^1E \rightarrow ^3A_2$; highlighted by blue background in Fig. 3). However, the existence of the singlet analog $^1E'$ has only been theoretically predicted to date.^{10,33} Nevertheless, as the group theory indicates that the energy level of $^1E'$ is commensurable with that of 3E , it is reasonable to assume that $^1E'$ is present in the TA spectrum. The $a_1 \rightarrow e$ transition produces another set of E

states, namely ${}^3E'$ and ${}^1E''$.

We got two triplet and three singlet excited states; however, the three ESA peaks in the singlet TA spectrum indicate that at least one doubly excited singlet state should also be accessible by absorption. Considering the possible second-order excitations, see the top of Fig. 3, energetically the double $a'_1 \rightarrow e$ process is the most favorable. According to the Kohn-Sham orbital picture, the energy demand of a double $a'_1 \rightarrow e$ excitation is similar to a single $a_1 \rightarrow e$ jump.

Altogether, chemical intuition and group theory strongly suggest that the additional states observed in TA spectroscopy are ${}^3E''$, ${}^1E'$, ${}^1A'_1$ and ${}^1E''$. These states are highlighted with red background in Fig. 3. Furthermore, given that only four defect-localized orbitals are present, any other possible distribution of electrons results in double excitations of significantly higher energy.

Now, we test the qualitative predictions of group theory by ab initio calculations. Our previously reported initial CASSCF-NEVPT2 results²⁶ indicated that the newly suggested states of ${}^3E''$, ${}^1E'$, ${}^1A'_1$, and ${}^1E''$ are located in the energy range of 3.3-4.6 eV relative to the ground triplet state (3A_2), which correspond well with our present measurement. Herein, we further investigate our hypothesis on ${}^3E''$, ${}^1E'$, ${}^1A'_1$, and ${}^1E''$ states by (i) a comparative analysis of CASSCF-NEVPT2 and CRPA+FCI, (ii) comparing theoretical oscillator strengths from CASSCF-NEVPT2 to the observed relative peak sizes.

As both theoretical approach takes state mixing effects into account, it is worth studying the composition of the eigenstates based on the group theoretically pure configurations of Fig. 3, see Tabs. S3-S4 of SI. Strikingly, state mixing effects are observed in all configurations of the singlet channel, in sharp contrast to the triplets where all states were found to be dominated by one configuration. For instance, we observe the previously reported¹⁶ presence of ${}^1E'$ in 1E , which enables the intersystem crossing to 3A_2 , as well as the previously reported^{19,60} significant contribution of ${}^1A'_1$ to the multireference wavefunction of 1A_1 . We emphasize here that the multireference character of singlets makes the single-determinant methods, such as DFT, highly unreliable for calculating energy differences.

Next, we turn our focus on excitation energies as summarized in Tab. I, left and visualized in Fig. 4; see also Tabs. S1-2 of SI for a detailed data analysis. With CASSCF-NEVPT2 we obtain triplet electronic energy levels of 2.11 eV (3E) and 4.34 eV (${}^3E''$), relative to the ground state, which corresponds to absorption peaks of 2.11 eV (${}^3A_2 \rightarrow {}^3E$) and 2.22 eV (${}^3E' \rightarrow {}^3E''$), respectively. The results agree well with the experimental peak positions of 1.95 eV and 2.39 eV, respectively. A similarly successful reproduction of the measured energy levels was achieved in the singlet channel, where the excited states are located, compared to the lowest-lying state of 1E , at 1.02 eV (1A_1), 2.73 eV (${}^1E'$), and 3.91 eV (${}^1A'_1$). The only outlier is the ${}^1E''$ state with 3.37 eV. Thus, within the measurement limit of <3.3 eV, we predict absorption at 1.02 eV (${}^1E \rightarrow {}^1A_1$) and 2.73 eV (${}^1E \rightarrow {}^1E'$) from the ground singlet state, while 1.71 eV (${}^1A_1 \rightarrow {}^1E'$), 2.89 eV (${}^1A_1 \rightarrow {}^1A'_1$) and 2.35 eV (${}^1A_1 \rightarrow {}^1E''$) from the first excited singlet.

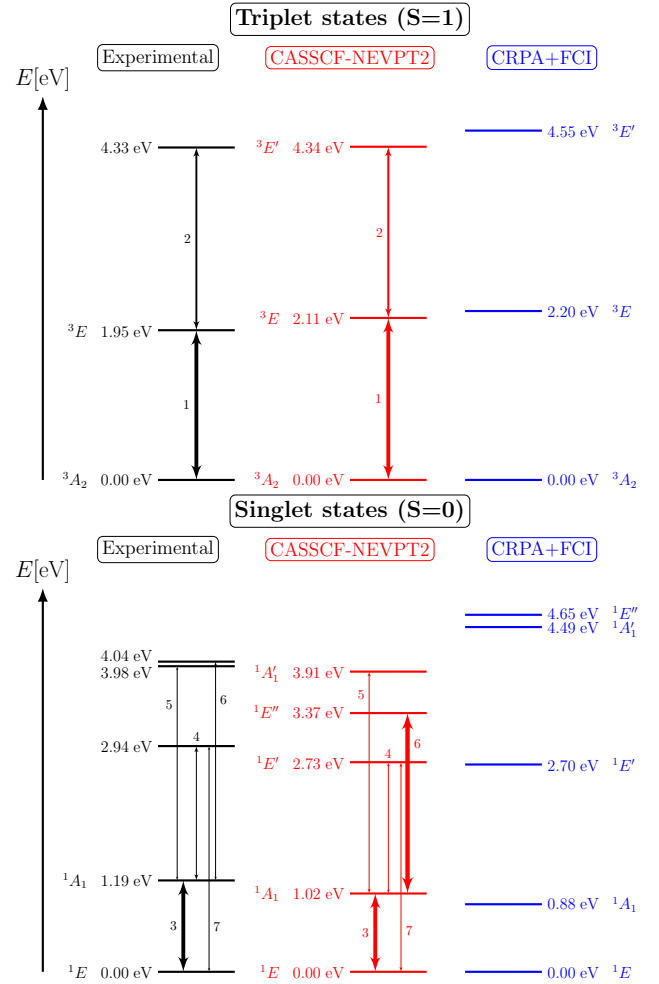


Figure 4. Comparison of experimental (black) and theoretical (red, blue) energy levels of the electronic states of NV^- in triplet (top graph) and singlet (bottom graph) spin state. Experimental levels were calculated from observed ZPL wavelengths, while theoretical values refer to vertical gaps, calculated at CASSCF-NEVPT2 and CI + CRPA level, respectively. (See SI, section S3.1 for a discussion of comparability of the three methods.) The thickness of arrows is proportional to the oscillator strength.

With cRPA+FCI the excitation energies in the triplet channel are 2.20 eV (${}^3A_2 \rightarrow {}^3E$) and 4.55 eV (${}^3A_2 \rightarrow {}^3E'$). The ${}^3E \rightarrow {}^3E'$ transition energy is at 2.35 eV. These energies agree very well with both experimental measurements and energies obtained with CASSCF-NEVPT2. For the singlet channel, the excitation energy to the first two states (1A_1 and ${}^1E'$) are at 0.88 eV and 2.70 eV, respectively. The next state is at 4.49 eV above the lowest singlet state (1E). This state is the ${}^1A'_1$ state, with the ${}^1E''$ state located 0.15 eV above the ${}^1A'_1$ state. This is in contrast to the position, ordering and splitting obtained with CASSCF-NEVPT2. The energy splitting of 0.15 eV between ${}^1A'_1$ and ${}^1E''$ is reminiscent of the energy splitting between the experimentally observed states at 3.98 eV and 4.04 eV, but the excitation energy is about 0.5 eV larger than experimentally observed. Furthermore, the ${}^1E''$ state described with cRPA+FCI is more than 1 eV above the value obtained with

Peak	Transition	Energy (eV)			Oscillator strength			DW (%)
		exp.	theory 1	theory 2	exp.	theory 1	theory 2	exp.
1	${}^3A_2 \rightarrow {}^3E$	1.945 [1.4]	2.11	2.20	1*	1	-	3.2 ^{61,62}
2	${}^3E \rightarrow {}^3E'$	2.385 [7.7]	2.22	2.35	0.49	0.54	-	8.1 ²⁸
3	${}^1E \rightarrow {}^1A_1$	1.19 [1.4]	1.02	0.88	1	1	-	41 ⁶²
4	${}^1A_1 \rightarrow {}^1E'$	1.75 [3.3]	1.71	1.82	0.22	0.04	-	42 ²⁸
5	${}^1A_1 \rightarrow {}^1E''/{}^1A'_1$	2.79 [6.9]	2.89	3.61	0.01	0.10	-	-
6	${}^1A_1 \rightarrow {}^1E''/{}^1A'_1$	2.85 [8.1]	2.35	3.77	0.02	1.14	-	-
7	${}^1E \rightarrow {}^1E'$	2.94 [4.7]	2.73	2.70	0.01	0.10	-	-

Table I. Summary of observed transition peak properties (Fig. 1b) compared to CASSCF-NEVPT2 (theory 1) and CRPA+FCI (theory 2) results. Transition energies are in eV, full-width-half-maximum (FWHM) of the experimental peaks (in square brackets) are measured in meV. Oscillator strengths of the singlet and the triplet systems are normalized to the corresponding ZPL cross-sections. *: Intensity halved assuming GSB and SE give equal contributions.

CASSCF-NEVPT2. The cRPA+FCI method involves certain approximations that may influence the positioning of energy levels. First, the electronic screening is in this case computed with the static dielectric function. Furthermore, in the present calculations, there are some double counting errors in the one-body matrix elements (Kohn-Sham energy levels) due to the exchange-correlation energy of the active space, which should be fully included in the two-body matrix elements, but which is neglected in this case. The present cRPA calculation, with the considered minimal basis set is qualitatively in agreement with experiments.

Altogether, CASSCF-NEVPT2 predicts the newly identified TA peak positions with less than 0.2 eV deviation from the measurement, with the exception of ${}^1E''$, which differs by 0.5 eV. This finding is strong evidence for the correctness of our assignment of higher-energy states shown in Fig. 3.

Apart from the transition energies, the transition oscillator strength (f_{osc}), i.e. absorption cross-section, could be used to determine the electronic states. (See SI, section S3.2 for details.) The calculated oscillator strengths, compared to the experimental integrated peak areas, are provided in Table I. The values are normalized, the same way as the experimental ones. In our comparison, we expect only an order-of-magnitude estimate from theory, given the approximations involved in our methods and the fact that the experimental values of f_{osc} are based only on ZPL peaks, even though the Debye-Waller factor could significantly vary.

In the triplet channel, we find $f_{\text{osc}} = 0.54$ for ${}^3E \rightarrow {}^3E'$ at CASSCF-NEVPT2 level, which is in good agreement with the experimental value of 0.49. In the singlet channel, the peak intensities show more variation. According to our theoretical calculations, after the ${}^1E \rightarrow {}^1A_1$ transition feature of the TA spectrum is the ${}^1A_1 \rightarrow {}^1E'$ transition ($f_{\text{osc}} = 0.04$), followed by the ${}^1E \rightarrow {}^1E'$ ($f_{\text{osc}} = 0.10$) and the ${}^1A_1 \rightarrow {}^1A'_1$ ($f_{\text{osc}} = 0.10$) transitions. The deviations of the oscillator strengths from the experimental values, 0.22, 0.01, and 0.01, respectively, are tolerable in these cases.

The ${}^1A_1 \rightarrow {}^1E''$ transition is an exceptional case, where the obtained f_{osc} value of 1.14 is almost two orders of magnitude higher than the experimental observations. Additionally, the

energy of the corresponding transition is in disagreement with the experimental results. This casts some doubt on the identity of one of the peaks at 2.79-2.85 eV, as such a deviation cannot likely be explained by DW-factor variations or by any factor neglected by our computational protocol (e.g. geometry relaxation effects). The potential causes of this discrepancy are discussed in the SI, section S3.3. For the cRPA+FCI calculations, the gauge for the position operator in the Wannier basis does not coincide with the center of charge density and hence the optical matrix elements and consequently the oscillator strengths are not evaluated with this level of theory.

In conclusion, our joint experimental and theoretical study elaborates on the high-energy spectra of the NV center in diamond. Our results, obtained through both TA spectroscopy and advanced computational methods, provide a comprehensive characterization of five high-energy states beyond the commonly studied optical cycle. By combining experimental transition energies and oscillator strengths with theoretical insights from CASSCF-NEVPT2 and cRPA+FCI methods, we not only provide the identification of these states but also deepen our understanding of the NV center's electronic structure.

These findings can have important implications for future applications of NV centers in quantum technologies, particularly in the development of more efficient spin-to-charge conversion readout mechanisms. Additionally, the results we obtained offer a valuable framework for benchmarking high-level first-principles methods in the study of point defects.

ACKNOWLEDGMENTS

This research was supported by the National Research, Development, and Innovation Office of Hungary within the Quantum Information National Laboratory of Hungary (Grant No. 2022-2.1.1-NL-2022-00004) and grants FK 135496 and FK 145395. Z.B. also acknowledges the financial support of the János Bolyai Research Fellowship of the Hungarian Academy of Sciences. We acknowledge the support of the European Union under Horizon Europe for the QRC-

4-ESP project (Grant Agreement 101129663), the QUEST project (Grant Agreement 101156088) and funding by the Max-Planck Society. C. L. acknowledges support provided by the Research Council of Norway and the University of Oslo through the research project QuTe (no. 325573, FriPro ToppForsk-program).

The computations were enabled by resources provided by the National Academic Infrastructure for Supercomputing in Sweden (NAISS) and the Swedish National Infrastructure for Computing (SNIC) at NSC, partially funded by the Swedish Research Council through grant agreement no. 2022-06725 and no. 2018-05973. We also acknowledge KIFŰ for awarding us computational resources at the Komondor supercomputer in Hungary. In addition, computations were performed on resources provided by UNINETT Sigma2 — the National Infrastructure for High Performance Computing and Data Storage in Norway.

REFERENCES

- ¹M. W. Doherty, N. B. Manson, P. Delaney, F. Jelezko, J. Wrachtrup, and L. C. Hollenberg, “The nitrogen-vacancy colour centre in diamond,” *Physics Reports* **528**, 1–45 (2013).
- ²C. L. Degen, F. Reinhard, and P. Cappellaro, “Quantum sensing,” *Rev. Mod. Phys.* **89**, 035002 (2017).
- ³J. F. Barry, J. M. Schloss, E. Bauch, M. J. Turner, C. A. Hart, L. M. Pham, and R. L. Walsworth, “Sensitivity optimization for NV-diamond magnetometry,” *Reviews of Modern Physics* **92**, 015004 (2020).
- ⁴N. Aslam, H. Zhou, E. K. Urbach, M. J. Turner, R. L. Walsworth, M. D. Lukin, and H. Park, “Quantum sensors for biomedical applications,” *Nature Reviews Physics* **5**, 157–169 (2023).
- ⁵S. Wehner, D. Elkouss, and R. Hanson, “Quantum internet: A vision for the road ahead,” *Science* **362** (2018), 10.1126/science.aam9288.
- ⁶G. Balasubramanian, P. Neumann, D. Twitchen, M. Markham, R. Kolesov, N. Mizuochi, J. Isoya, J. Achard, J. Beck, J. Tissler, V. Jacques, P. R. Hemmer, F. Jelezko, and J. Wrachtrup, “Ultralong spin coherence time in isotopically engineered diamond,” *Nat. Mater.* **8**, 383 (2009).
- ⁷J. Michl, J. Steiner, A. Denisenko, A. Bülow, A. Zimmermann, K. Nakamura, H. Sumiya, S. Onoda, P. Neumann, J. Isoya, and J. Wrachtrup, “Robust and Accurate Electric Field Sensing with Solid State Spin Ensembles,” *Nano Letters* **19**, 4904–4910 (2019), publisher: American Chemical Society.
- ⁸G. Kucsko, P. C. Maurer, N. Y. Yao, M. Kubo, H. J. Noh, P. K. Lo, H. Park, and M. D. Lukin, “Nanometre-scale thermometry in a living cell,” *Nature* **500**, 54–58 (2013).
- ⁹P. Ouartchaiyapong, K. W. Lee, B. A. Myers, and A. C. B. Jayich, “Dynamic strain-mediated coupling of a single diamond spin to a mechanical resonator,” *Nature Communications* **5**, 4429 (2014), number: 1 Publisher: Nature Publishing Group.
- ¹⁰Ádám Gali, “Ab initio theory of the nitrogen-vacancy center in diamond,” *Nanophotonics* **8**, 1907–1943 (2019).
- ¹¹A. Gali, E. Jánzén, P. Deák, G. Kresse, and E. Kaxiras, “Theory of spin-conserving excitation of the $n-v^-$ center in diamond,” *Phys. Rev. Lett.* **103**, 186404 (2009).
- ¹²P. Delaney, J. C. Greer, and J. A. Larsson, “Spin-polarization mechanisms of the nitrogen-vacancy center in diamond,” *Nano Letters* **10**, 610–614 (2010), <https://doi.org/10.1021/nl903646p>.
- ¹³Y. Ma, M. Rohlfing, and A. Gali, “Excited states of the negatively charged nitrogen-vacancy color center in diamond,” *Phys. Rev. B* **81**, 041204 (2010).
- ¹⁴S. Choi, M. Jain, and S. G. Louie, “Mechanism for optical initialization of spin in nv^- center in diamond,” *Phys. Rev. B* **86**, 041202 (2012).
- ¹⁵G. Thiering and A. Gali, “Ab initio calculation of spin-orbit coupling for an NV center in diamond exhibiting dynamic jahn-teller effect,” *Physical Review B* **96**, 081115 (2017).
- ¹⁶G. Thiering and A. Gali, “Theory of the optical spin-polarization loop of the nitrogen-vacancy center in diamond,” *Phys. Rev. B* **98**, 085207 (2018).
- ¹⁷M. Bockstedte, F. Schütz, T. Garratt, V. Ivády, and A. Gali, “Ab initio description of highly correlated states in defects for realizing quantum bits,” *npj Quantum Materials* **3**, 31 (2018).
- ¹⁸H. Ma, M. Govoni, and G. Galli, “Quantum simulations of materials on near-term quantum computers,” *npj Computational Materials* **6**, 85 (2020).
- ¹⁹C. Bhandari, A. L. Wysocki, S. E. Economou, P. Dev, and K. Park, “Multiconfigurational study of the negatively charged nitrogen-vacancy center in diamond,” *Phys. Rev. B* **103**, 014115 (2021).
- ²⁰N. Sheng, C. Vorwerk, M. Govoni, and G. Galli, “Green’s function formulation of quantum defect embedding theory,” *Journal of Chemical Theory and Computation* **18**, 3512–3522 (2022), pMID: 35648660, <https://doi.org/10.1021/acs.jctc.2c00240>.
- ²¹B. A. Barker and D. A. Strubbe, “Spin-flip bethe-salpeter equation approach for ground and excited states of open-shell molecules and defects in solids,” (2022), arXiv:2207.04549 [cond-mat.mtrl-sci].
- ²²S. Haldar, A. Mitra, M. R. Hermes, and L. Gagliardi, “Local excitations of a charged nitrogen vacancy in diamond with multireference density matrix embedding theory,” *The Journal of Physical Chemistry Letters* **14**, 4273–4280 (2023), pMID: 37126760, <https://doi.org/10.1021/acs.jpcclett.3c00551>.
- ²³A. V. Ivanov, Y. L. A. Schmerwitz, G. Levi, and H. Jónsson, “Electronic excitations of the charged nitrogen-vacancy center in diamond obtained using time-independent variational density functional calculations,” *SciPost Phys.* **15**, 009 (2023).
- ²⁴Y. Chen, T. Jiang, H. Chen, E. Han, A. Alavi, K. Yu, E. Wang, and J. Chen, “Multiconfigurational nature of electron correlation within nitrogen-vacancy centers in diamond,” *Phys. Rev. B* **108**, 045111 (2023).
- ²⁵K. Li, V. D. Dergachev, I. D. Dergachev, S. Zhang, S. A. Varganov, and Y. Ping, “Excited-state dynamics and optically detected magnetic resonance of solid-state spin defects from first principles,” *Phys. Rev. B* **110**, 184302 (2024).
- ²⁶Z. Benedek, Ádám Ganyecz, A. Pershin, V. Ivády, and G. Barcza, “Accurate and convergent energetics of color centers by wavefunction theory,” (2024), arXiv:2406.05092 [cond-mat.mtrl-sci].
- ²⁷M. Gulka, D. Wirtitsch, V. Ivády, J. Vodník, J. Hruby, G. Magchiels, E. Bourgeois, A. Gali, M. Trupke, and M. Nešladek, “Room-temperature control and electrical readout of individual nitrogen-vacancy nuclear spins,” *Nature Communications* **12**, 4421 (2021), bandiera_abtest: a Cc_license_type: cc_by Cg_type: Nature Research Journals Number: 1 Primary_atype: Research Publisher: Nature Publishing Group Subject_term: Optical properties of diamond;Electronic properties and materials;Quantum information;Qubits Subject_term_id: diamond;electronic-properties-and-materials;quantum-information;qubits.
- ²⁸M.-T. Luu, A. Tayefeh Younesi, and R. Ulbricht, “Nitrogen-vacancy centers in diamond: discovery of additional electronic states,” *Materials for Quantum Technology* (2024).
- ²⁹A. T. Younesi and R. Ulbricht, “Broadband transient absorption spectroscopy using an incoherent white-light source as probe,” *Opt. Express* **30**, 38896–38906 (2022).
- ³⁰A. S. Zyubin, A. M. Mebel, M. Hayashi, H. C. Chang, and S. H. Lin, “Quantum chemical modeling of photoadsorption properties of the nitrogen-vacancy point defect in diamond,” *Journal of Computational Chemistry* **30**, 119–131 (2009), <https://onlinelibrary.wiley.com/doi/pdf/10.1002/jcc.21042>.
- ³¹J. R. Maze, A. Gali, E. Togan, Y. Chu, A. Trifonov, E. Kaxiras, and M. D. Lukin, “Properties of nitrogen-vacancy centers in diamond: the group theoretic approach,” *New Journal of Physics* **13**, 025025 (2011).
- ³²M. W. Doherty, N. B. Manson, P. Delaney, and L. C. L. Hollenberg, “The negatively charged nitrogen-vacancy center in diamond: the electronic solution,” *New Journal of Physics* **13**, 025019 (2011).
- ³³D. Wirtitsch, G. Wachter, S. Reisenbauer, M. Gulka, V. Ivády, F. Jelezko, A. Gali, M. Nešladek, and M. Trupke, “Exploiting ionization dynamics in the nitrogen vacancy center for rapid, high-contrast spin, and charge state initialization,” *Phys. Rev. Res.* **5**, 013014 (2023).
- ³⁴P. Siegbahn, A. Heiberg, B. Roos, and B. Levy, “A comparison of the super-ci and the newton-raphson scheme in the complete active space scf method,” *Physica Scripta* **21**, 323 (1980).
- ³⁵B. O. Roos, P. R. Taylor, and P. E. Siegbahn, “A complete active space

- scf method (casscf) using a density matrix formulated super-ci approach,” *Chemical Physics* **48**, 157–173 (1980).
- ³⁶P. E. M. Siegbahn, J. Almlöf, A. Heiberg, and B. O. Roos, “The complete active space SCF (CASSCF) method in a Newton–Raphson formulation with application to the HNO molecule,” *The Journal of Chemical Physics* **74**, 2384–2396 (1981), https://pubs.aip.org/aip/jcp/article-pdf/74/4/2384/18926917/2384_1_online.pdf.
- ³⁷C. Angeli, R. Cimiraglia, S. Evangelisti, T. Leininger, and J.-P. Malrieu, “Introduction of n-electron valence states for multireference perturbation theory,” *The Journal of Chemical Physics* **114**, 10252–10264 (2001).
- ³⁸C. Angeli, R. Cimiraglia, and J.-P. Malrieu, “n-electron valence state perturbation theory: A spinless formulation and an efficient implementation of the strongly contracted and of the partially contracted variants,” *The Journal of Chemical Physics* **117**, 9138–9153 (2002), <https://doi.org/10.1063/1.1515317>.
- ³⁹C. Angeli, M. Pastore, and R. Cimiraglia, “New perspectives in multireference perturbation theory: the n-electron valence state approach,” *Theoretical Chemistry Accounts* **117**, 743–754 (2007).
- ⁴⁰L. Muechler, D. I. Badrtidinov, A. Hampel, J. Cano, M. Rösner, and C. E. Dreyer, “Quantum embedding methods for correlated excited states of point defects: Case studies and challenges,” *Phys. Rev. B* **105**, 235104 (2022).
- ⁴¹T. H. Dunning, “Gaussian basis sets for use in correlated molecular calculations. i. the atoms boron through neon and hydrogen,” *The Journal of Chemical Physics* **90**, 1007–1023 (1989), <https://doi.org/10.1063/1.456153>.
- ⁴²F. Weigend, “Accurate coulomb-fitting basis sets for h to rn,” *Phys. Chem. Chem. Phys.* **8**, 1057–1065 (2006).
- ⁴³F. Weigend, A. Köhn, and C. Hättig, “Efficient use of the correlation consistent basis sets in resolution of the identity MP2 calculations,” *The Journal of Chemical Physics* **116**, 3175–3183 (2002), https://pubs.aip.org/aip/jcp/article-pdf/116/8/3175/19300676/3175_1_online.pdf.
- ⁴⁴F. Neese, “An improvement of the resolution of the identity approximation for the formation of the coulomb matrix,” *J. Comp. Chem.* **24**, 1740–1747 (2003).
- ⁴⁵F. Neese, F. Wennmohs, A. Hansen, and U. Becker, “Efficient, approximate and parallel hartree-fock and hybrid dft calculations. a ‘chain-of-spheres’ algorithm for the hartree-fock exchange,” *Chem. Phys.* **356**, 98–109 (2009).
- ⁴⁶B. Helmich-Paris, B. de Souza, F. Neese, and R. Izsák, “An improved chain of spheres for exchange algorithm,” *J. Chem. Phys.* **155**, 104109 (2021).
- ⁴⁷F. Neese, “Software update: the orca program system, version 5.0,” *WIREs Comput. Molec. Sci.* **12**, e1606 (2022).
- ⁴⁸C. Kollmar, K. Sivalingam, B. Helmich-Paris, C. Angeli, and F. Neese, “A perturbation-based super-ci approach for the orbital optimization of a casscf wave function,” *J. Comput. Chem.* **40**, 1463–1470 (2019).
- ⁴⁹F. Neese, “The shark integral generation and digestion system,” *J. Comp. Chem.* , 1–16 (2022).
- ⁵⁰G. Kresse and J. Hafner, “Ab initio molecular-dynamics simulation of the liquid-metal–amorphous-semiconductor transition in germanium,” *Phys. Rev. B* **49**, 14251–14269 (1994).
- ⁵¹G. Kresse and J. Furthmüller, “Efficient iterative schemes for *ab initio* total-energy calculations using a plane-wave basis set,” *Phys. Rev. B* **54**, 11169–11186 (1996).
- ⁵²J. Heyd, G. E. Scuseria, and M. Ernzerhof, “Hybrid functionals based on a screened coulomb potential,” *J. Chem. Phys.* **118**, 8207 (2003).
- ⁵³J. Heyd, G. E. Scuseria, and M. Ernzerhof, “Erratum: “hybrid functionals based on a screened coulomb potential” [*J. Chem. Phys.* **118**, 8207 (2003)],” *J. Chem. Phys.* **124**, 219906 (2006).
- ⁵⁴F. Aryasetiawan, M. Imada, A. Georges, G. Kotliar, S. Biermann, and A. I. Lichtenstein, “Frequency-dependent local interactions and low-energy effective models from electronic structure calculations,” *Phys. Rev. B* **70**, 195104 (2004).
- ⁵⁵K. Beha, A. Batalov, N. B. Manson, R. Bratschitsch, and A. Leitenstorfer, “Optimum photoluminescence excitation and recharging cycle of single nitrogen-vacancy centers in ultrapure diamond,” *Physical review letters* **109**, 097404 (2012).
- ⁵⁶R. Ulbricht and Z.-H. Loh, “Excited-state lifetime of the nv- infrared transition in diamond,” *Physical Review B* **98**, 094309 (2018).
- ⁵⁷A. Gali, M. Fyta, and E. Kaxiras, “Ab initio supercell calculations on nitrogen-vacancy center in diamond: Electronic structure and hyperfine tensors,” *Physical Review B—Condensed Matter and Materials Physics* **77**, 155206 (2008).
- ⁵⁸J. A. Larsson and P. Delaney, “Electronic structure of the nitrogen-vacancy center in diamond from first-principles theory,” *Phys. Rev. B* **77**, 165201 (2008).
- ⁵⁹A. Gali, E. Janzén, P. Deák, G. Kresse, and E. Kaxiras, “Theory of spin-conserving excitation of the $n - V^-$ center in diamond,” *Phys. Rev. Lett.* **103**, 186404 (2009).
- ⁶⁰K. Li, V. D. Dergachev, I. D. Dergachev, S. Zhang, S. A. Varganov, and Y. Ping, “Excited-state dynamics and optically detected magnetic resonance of solid-state spin defects from first principles,” (2024), [arXiv:2404.05917 \[cond-mat.mtrl-sci\]](https://arxiv.org/abs/2404.05917).
- ⁶¹A. Alkauskas, B. B. Buckley, D. D. Awschalom, and C. G. Van de Walle, “First-principles theory of the luminescence lineshape for the triplet transition in diamond nv centres,” *New Journal of Physics* **16**, 073026 (2014).
- ⁶²P. Kehayias, M. Doherty, D. English, R. Fischer, A. Jarmola, K. Jensen, N. Leefer, P. Hemmer, N. Manson, and D. Budker, “Infrared absorption band and vibronic structure of the nitrogen-vacancy center in diamond,” *Physical Review B—Condensed Matter and Materials Physics* **88**, 165202 (2013).